Asociación Argentina
de Mecánica Computacional

Mecánica Computacional Vol XXXI, págs. 735-750 (artículo completo)
Alberto Cardona, Paul H. Kohan, Ricardo D. Quinteros, Mario A. Storti (Eds.)
Salta, Argentina, 13-16 Noviembre 2012

THREE-DIMENSIONAL FREE SURFACE FLOWS WITH ABSORBING BOUNDARY CONDITIONS

Laura Battaglia[a,b], Mario A. Storti[a], Rodrigo R. Paz[a] and Jorge D'Elía[a]

[a]*Centro Internacional de Métodos Computacionales en Ingeniería (CIMEC)*
Instituto de Desarrollo Tecnológico para la Industria Química (INTEC)
Universidad Nacional del Litoral - CONICET Güemes 3450, 3000-Santa Fe, Argentina
e-mail: lbattaglia@santafe-conicet.gob.ar, (mstorti,rodrigop,jdelia)@intec.unl.edu.ar
web page: http://www.cimec.org.ar

[b]*Grupo de Investigación en Métodos Numéricos en Ingeniería (GIMNI)*
Universidad Tecnológica Nacional - Facultad Regional Santa Fe
Lavaise 610, 3000-Santa Fe, Argentina

Keywords: fluid mechanics, free surface, arbitrary Lagrangian-Eulerian method, artificial boundaries, absorbing layer.

Abstract. The free surface incompressible fluid flow is solved through an arbitrary Lagrangian-Eulerian strategy, considering a deformable single-phase domain with an artificial boundary, which is managed through an absorbing technique for avoiding spurious wave reflections at the contour. This absorbing strategy is based on the shallow water approximation, as introduced in previous works (*Absorbing Boundary Conditions for Free-Surface Flows in Open Domains*, Storti, M., Battaglia, L., Paz, R., and D'Elía, J., 10th World Congress on Computational Mechanics - WCCM 2012; *Interface-Tracking Free-Surface Flows in Open Domains*, Battaglia, L., Storti, M. and D'Elía, J., Mecánica Computacional Vol. XXX, pp. 2209-2223). The resolution scheme consists of three numerical stages: (i) the fluid flow stage, where the incompressible Navier-Stokes equations for viscous fluid flows are solved; (ii) the free surface transport; and (iii) the mesh movement, solved as a pseudo-elastic problem. The strategy is used for solving some three-dimensional free-surface flows in domains with at least one artificial boundary, emphasizing the effect of the proposed absorbing layer.

1 INTRODUCTION

The Free-Surface (FS) incompressible fluid flow problems involve a wide range of engineering problems. Some of these problems correspond to the fluid flow in closed recipients, as tanks (Battaglia et al., 2012), while some others count either on inflow and outflow sections, as open channels (Güler et al., 1999), or constitute a part of infinite -or semi-infinite- problems, as in coastal or off-shore simulations. In the case of open domains, boundary conditions to be imposed to artificial boundaries for performing numerical simulations are not always the typical ones. For example, for a subcritical flow in an open channel with a FS, the characteristics reflected on an artificial outflow sections with boundary conditions over the pressure can travel upstream, affecting the flow patterns with non-physical waves.

For overcoming the non-physical reflections of surface waves in FS fluid flows in open domains, it is a common practice to impose absorbing boundary condition or non-reflective boundary conditions in the numerical models of the problems. These issues are also frequent in other hyperbolic problems, as in compressible fluid flows (Storti et al., 2008) or channel flows represented by the shallow water equations (Paz et al., 2011). Other strategies are applied over regions that are close to the artificial contours, constituting an Absorbing Layer (AL), a sponge, or a buffer zone, among others (Colonius, 2004).

In a previous work, a local AL was proposed for two-dimensional (2D) open domains without mean current (Battaglia et al., 2011). In the present work, the extension to three-dimensional (3D) fluid flow cases with artificial boundaries is shown, as part of an arbitrary Lagrangian-Eulerian (ALE) methodology for solving FS flow problems, which is an interface-tracking approach where the FS constitutes one of the frontiers of the domain and a single fluid is considered (Hughes et al., 1981; Battaglia et al., 2006). Numerical examples are presented.

The numerical method is implemented as part of the general-purpose libraries of the PETSc-FEM code (PETSc-FEM, 2012), that is based on the Message Passing Interface (MPI, 2012) and the Portable Extensible Toolkit for Scientific Computation (PETSc) libraries (Balay et al., 2008) for parallel computing. The numerical results were obtained using the Coyote Cluster at CIMEC.

2 GOVERNING EQUATIONS

The resolution of the FS fluid flows within the ALE approach is performed here as a sequence of stages in each time step, which are: i) the resolution of the Navier-Stokes (NS) equations for the fluid state; ii) the determination of the FS position, given by the new nodal coordinates of the FS nodes, determined by a transport equation; iii) the mesh update procedure, that consists of adapting the mesh to the new domain shape, keeping the topology. Each stage is separately described in the following sections.

The first and the third stages are performed over the same mesh topology; the second one is solved over the faces that constitute the FS, which is a 2D tessellation when the problem is 3D, or one-dimensional mesh for a 2D fluid flow problem.

2.1 Fluid flow with a free surface

The ALE approach for the NS equations consists of solving the following equations over the fluid domain $\Omega = \Omega(t)$,

$$\rho\left(\partial_t \mathbf{u} + \mathbf{c}\cdot\nabla\mathbf{u} - \mathbf{f}\right) - \nabla\cdot\boldsymbol{\sigma} = 0\,; \tag{1}$$

$$\nabla\cdot\mathbf{u} = 0\,, \tag{2}$$

for time $t \in [0, T]$, with T a final time, where $\mathbf{u}$ is the fluid velocity, $\mathbf{f}$ the body force, ρ the fluid density, and $\boldsymbol{\sigma} = \boldsymbol{\sigma}(\mathbf{u}, p)$ is the fluid stress tensor,

$$\boldsymbol{\sigma} = -p\mathbf{I} + \mathbf{T} \; ; \tag{3}$$

being p the pressure, $\mathbf{I}$ the identity tensor, and

$$\mathbf{T} = 2\mu\boldsymbol{\epsilon}(\mathbf{u}) \; ; \tag{4}$$

the deviatoric part of $\boldsymbol{\sigma}$, that depends on the dynamic viscosity μ, and on the strain rate

$$\boldsymbol{\epsilon}(\mathbf{u}) = \frac{1}{2}(\nabla\mathbf{u} + \nabla^T\mathbf{u}) \; . \tag{5}$$

The convective velocity $\mathbf{c}$ for the advective term of Eq. (1) is defined as

$$\mathbf{c} := \mathbf{u} - \hat{\mathbf{u}}; \tag{6}$$

with $\hat{\mathbf{u}}$ the mesh velocity determined from the update of the nodal positions due to the deformation of the domain in each time step.

The boundary conditions for the contour of the domain $\partial\Omega = \Gamma$ are

$$\mathbf{v} = \mathbf{v}_\mathrm{D} \qquad \text{on } \Gamma_\mathrm{D} \; ; \tag{7}$$

$$\boldsymbol{\sigma} \cdot \mathbf{n} = \mathbf{t} \qquad \text{on } \Gamma_\mathbf{t} \; ; \tag{8}$$

where velocities are given for the Dirichlet part Γ_D, e.g. over solid walls, while $\Gamma_\mathbf{t}$ involves the interfaces between fluids or, particularly, a FS. Note that $\Gamma = \Gamma_\mathrm{D} \cup \Gamma_\mathbf{t}$ and $\Gamma_\mathrm{D} \cap \Gamma_\mathbf{t} = \emptyset$.

The boundary condition for a FS, with $\Gamma_\mathbf{t} = \Gamma_\mathrm{FS}$, represents the equilibrium between the projections of the stress tensors from the liquid and from the gas, $\boldsymbol{\sigma}_l$ and $\boldsymbol{\sigma}_g$, respectively,

$$\boldsymbol{\sigma}_l \cdot \mathbf{n} = \boldsymbol{\sigma}_g \cdot \mathbf{n} \qquad \text{on } \Gamma_\mathrm{FS}. \tag{9}$$

From the definition of the stress tensor in a fluid, Eqs. (3,4), and neglecting the viscosity and the density of the gaseous phase, then $\boldsymbol{\sigma} = -p\mathbf{I}$. If the pressure over the interface is the atmospheric pressure, i.e. $p = P_\mathrm{atm}$, it results $\mathbf{t} = -P_\mathrm{atm}\,\mathbf{n}$ on Γ_FS.

The AL is defined over part of the fluid domain, as a strip of elements close to the artificial boundary, where the Eqs. (1,2) include additional terms described in Sec. 3.

A finite element method implemented in the PETSc-FEM (2012) code is used for the discretization and resolution of the system of Eqs. (1,2). As the interpolations for the velocity and the pressure fields are equal, streamline upwind/Petrov-Galerkin (SUPG) (Brooks and Hughes, 1982) and pressure stabilizing/Petrov-Galerkin (PSPG) (Tezduyar et al., 1992) stabilization procedures are used for avoiding numerical instabilities.

2.2 Free surface movement

The FS is defined over faces of elements for the 3D case, or sides for 2D flows. The movement of the FS is given for the displacement of the corresponding nodes, which in this approach are measured over fixed directions, that for each FS node is represented by a unit vector $\hat{\mathbf{s}}_j$ (Battaglia et al., 2006). Then, the position of the FS node j in time t can be written as

$$\mathbf{x}_j(t) = \mathbf{x}_{0,j} + \eta_j(t)\,\hat{\mathbf{s}}_j \; ; \tag{10}$$

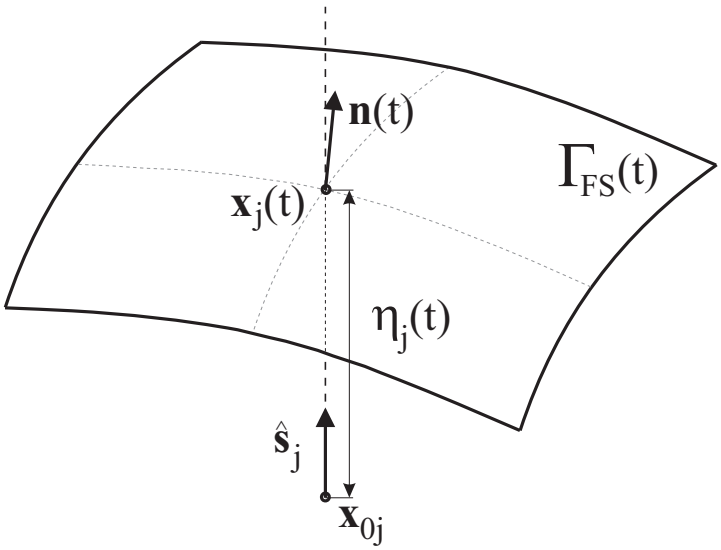

Figure 1: Free surface nodal displacements.

with $\mathbf{x}_{0,j}$ the initial position of the j-node. The scalar η_j represents the elevation of the j-node with respect to $\mathbf{x}_{0,j}$ along the direction $\hat{\mathbf{s}}_j$, see Fig. 1. For using Eq. (10), η_j has to be calculated from the kinematic FS condition,

$$\mathbf{u} \cdot \mathbf{n} = \partial_t \boldsymbol{\eta} \cdot \mathbf{n} \quad \text{over } \Gamma_{\text{FS}}; \tag{11}$$

with $\boldsymbol{\eta} = \eta\, \hat{\mathbf{s}}$ the elevation (vector) of the FS. As $\hat{\mathbf{s}}$ is constant, then

$$\partial_t \eta = \frac{\mathbf{u} \cdot \mathbf{n}}{\hat{\mathbf{s}} \cdot \mathbf{n}}\,. \tag{12}$$

For the general case of 3D fluid flows, and adopting $\hat{\mathbf{s}} \parallel x_3$, the scalar FS elevation can be represented as $\eta = \eta(x_1, x_2, t)$, so that the implicit expression is

$$F(\mathbf{x}, t) = x_3 - \eta = 0. \tag{13}$$

Considering that the unit vector normal to the FS is $\mathbf{n} = \nabla F(\mathbf{x})$, and replacing in Eq. (12), an advection equation in η arises,

$$\partial_t \eta = \frac{1}{H} \mathbf{u} \cdot \mathbf{n}\,; \tag{14}$$

where $H = \hat{\mathbf{s}} \cdot \mathbf{n}$ is a projection parameter. Re-arranging and operating, it leads to the following time-dependent transport problem in η,

$$\partial_t \eta + \mathbf{u}_{\parallel} \cdot \hat{\nabla} \eta = s \qquad \text{in } \Omega'_{\text{FS}}\,; \tag{15}$$

$$\eta = \eta_{\text{D}} \qquad \text{over } \Gamma'_{\text{D}}\,; \tag{16}$$

with the source term $s = u_3/H$ representing the fluid velocity component in the direction of $\hat{\mathbf{s}}$, and $\mathbf{u}_{\parallel} = H^{-1}\ [u_1; u_2]^T$ the fluid velocity in the FS reference plane. The domain $\Omega'_{\text{FS}} = \Gamma_{\text{FS}}$ has $n_{\text{dim}} - 1$ spatial dimensions, with n_{dim} the spatial dimensions in the flow problem. As Eq. (15) is hyperbolic, Dirichlet boundary conditions are given in inflow sections, if these exist, which means that $\Gamma'_{\text{D}} = \{\Gamma'_{\text{FS}} \mid \mathbf{u}_{\parallel} \cdot \hat{\mathbf{n}} < 0\}$.

The numerical solution of Ecs. (15,16) through a Galerkin procedure requires a stabilization when advective terms are dominant. In particular, a SUPG (Brooks and Hughes, 1982) stabilization is chosen. For 2D cases, there is an ad-hoc procedure for solving the system of equations, while the FS for 3D cases is solved with the advective-diffusive module of PETSc-FEM (2012).

Note that only the FS nodes move with this strategy, while the nodes inside $\Omega(t)$ are displaced using an auxiliary strategy that is independent of the fluid dynamics, see Sec. 2.3.

2.3 Mesh update

Once the new position of the FS is known, there is a change in the shape of the fluid domain $\Omega(t)$, and the mesh has to be modified to fit it. There are different methodologies to account for the shape change, such as remeshing, that is usually expensive, or some procedures for relocating the entities of the mesh without changing the topology.

In this approach, the mesh update is performed as a relocalization of the mesh nodes by a pseudo-elastic problem, in which the FS displacements constitute imposed displacements. Then, the third stage is solved as an elastic problem with imposed boundary displacements by using the elastic solver of the PETSc-FEM (2012) code, considering a linear elastic artificial material with an elasticity module and a Poisson coefficient arbitrary chosen. This strategy is appropriate for small to moderate FS displacements; otherwise, more elaborated procedures should be employed, such as the proposed by López et al. (2007), which is also implemented in PETSc-FEM.

3 ABSORBING LAYER

The AL strategy is based on a similar one proposed for the shallow water (SW) equations (Storti, 2011), that for a one-dimensional domain are

$$\partial_t h + \partial_x (uh) = 0; \tag{17}$$

$$\partial_t hu + \partial_x \left(\frac{1}{2} u^2 + gh \right) = -g\, \partial_x H. \tag{18}$$

where u is the mean horizontal velocity, h is the height of the fluid, g is the gravity acceleration, and the height of the bottom is expressed by $H = H(x)$. The well-known characteristic velocities for this system are $u + c$ and $u - c$, where $c = \sqrt{gh}$.

In the case of subcritical flows, a fraction of the waves reflect on the artificial boundary and travel upstreams with velocity $u - c$, perturbing the flow inside the domain. By performing an eigenvalue decomposition of the Jacobian of the flux and taking as a reference a mean fluid depth h_o, a mean horizontal velocity u_0, and a mean c_0, an absorbing term is defined in each of the Eqs. (17,18), giving for a constant H the following system (Battaglia et al., 2011),

$$\partial_t h + \partial_x (uh) - K\, h_0\, (u_0 - c_0) \left\{ \frac{h - h_0}{h_0} - \frac{u - u_0}{u_0} \right\} = 0; \tag{19}$$

$$\partial_t hu + \partial_x \left(\frac{1}{2} u^2 + gh \right) + K\, c_0\, (u_0 - c_0) \left\{ \frac{h - h_0}{h_0} - \frac{u - u_0}{u_0} \right\} = 0; \tag{20}$$

where K is a penalization parameter. The last terms in Eqs. (19,20) perform the absorption of the reflected spurious waves.

In the ALE-FS methodology, the parameters involved in the equations are not the same as in SW; then, an equivalence between both approaches has to be established, taking into account that will be applied only over the AL and not over the whole fluid domain.

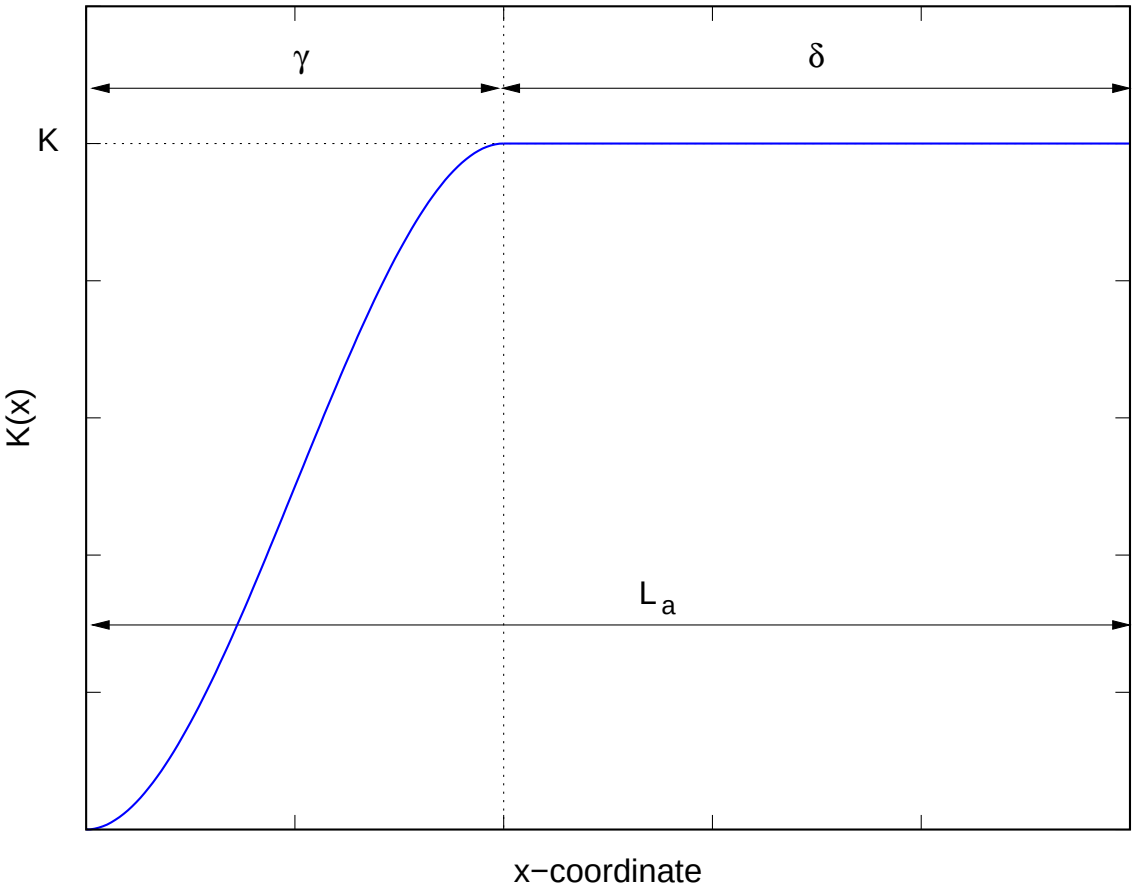

Figure 2: Variation of the penalty parameter K along the absorbing layer of length L_a.

In general, the horizontal velocity u is not uniform in the depth of the flow for NS; however, in each element, a mean velocity can be adopted for replacing u in Eqs. (19,20). In the case of u_0, for quasi-steady conditions in the fluid flow, it is usually an input data for the computation.

With respect to the depths involved in the absorbing term, h_0 is also an input data, while the numerator of the h-term is determined from the information given in the NS model. Considering the wave expression from the potential theory, together with the Bernoulli equation and other appropriate considerations (Battaglia et al., 2011), then

$$\eta = h - h_0 \approx \frac{p - P_{\text{atm}}}{\rho\, g} + (z - z_0). \tag{21}$$

where $z = 0$ corresponds to the bottom, z is the vertical position, and p is the value of the pressure, the last two measured in each Gauss point.

The transition from the region where the ALE-NS equations are solved to the one with absorbing terms has to be smooth in order to avoid reflected waves in the frontier between these regions (Clément, 1996). This can be made by choosing a spatial variation for the penalization parameter, as a function of the x-coordinate, i.e. $\mathrm{K} = \mathrm{K}(x)$, such that the AL is divided in two regions, as represented in Fig. 2. The first one, indicated with γ in such figure, presents a cubic variation of K, from $\mathrm{K} = 0$ to the maximum K imposed. In the other region, δ in Fig. 2, K takes the constant maximum value.

4 NUMERICAL EXAMPLES

The numerical examples consists of three dimensional domains with a wave generator region. In each case, the wave generation is given by the horizontal component of the gravity vector $\mathbf{g} = [g_x \;\; g_y \;\; g_z] = [g_x(t) \;\; 0 \;\; g_v]$, where g_v is the vertical magnitude of the gravity, and

$$g_x = A\, g_v \;\sin(\omega t); \tag{22}$$

where A is the non-dimensional amplitude, $\omega = 2\pi$ is the imposed circular frequency and t is the time. The resulting wavelength is $\lambda = 3.873$ m. The fluid flow is considered Newtonian and incompressible in all of the examples.

The decay of the wave amplitude A_w in the cases with AL can be estimated as

$$A_w(x) \propto \exp^{-\int K(x)\, \mathrm{dx}}, \tag{23}$$

where $A_w(x)$ is the wave amplitude, and

$$\int K(x)\, \mathrm{dx} = \int (3x^2 - 2x^3)\, \mathrm{dx} = \mathrm{x}^3 - \frac{\mathrm{x}^4}{2}, \tag{24}$$

that is valid for the transition region of the absorbing part.

4.1 Three dimensional open channel with waves generator

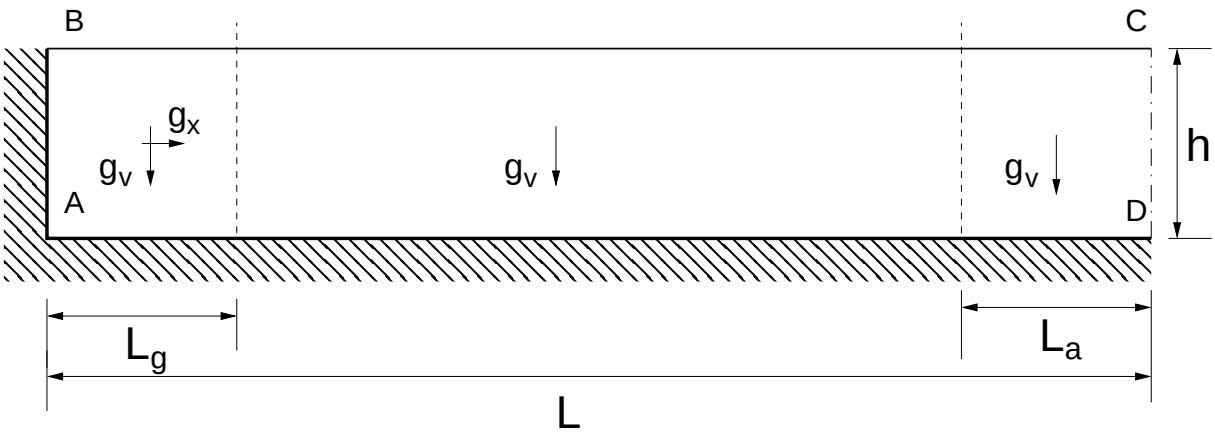

Figure 3: Three dimensional open channel. Domain geometry.

The open channel dimensions are length $L = 20$ m, water depth of $h = 1$ m, width $W = 0.5$ m, and the waves are generated over the $L_g = 1.9365$ m section, see Fig. 3. Perfect slip boundary conditions $\mathbf{u} \cdot \hat{\mathbf{n}} = 0$, with $\hat{\mathbf{n}}$ the unit vector normal to the walls, are given in the sides AB, AD and CD. In particular, CD constitutes the artificial boundary. Over the free surface, BC, the condition $P_{\text{atm}} = 0$ is adopted. Equal values of the variables are imposed between the two longitudinal-vertical faces parallel to the ABCD plane indicated in Fig. 3.

The kinematic viscosity of the fluid is $\nu = 1 \times 10^{-5}$ m^{2}s^{-1}, and the fluid density is $\rho = 1$ kg m^{-3}. The vertical gravity acceleration is $g_v = 1$ m s^{-2}, and a non-dimensional amplitude $A = 0.02$ is adopted for determining g_x from Eq. (22). Furthermore, the wave propagation velocity is $c = \sqrt{g_v\, h} = 1$ m s^{-1}.

The problem was solved in three different conditions:

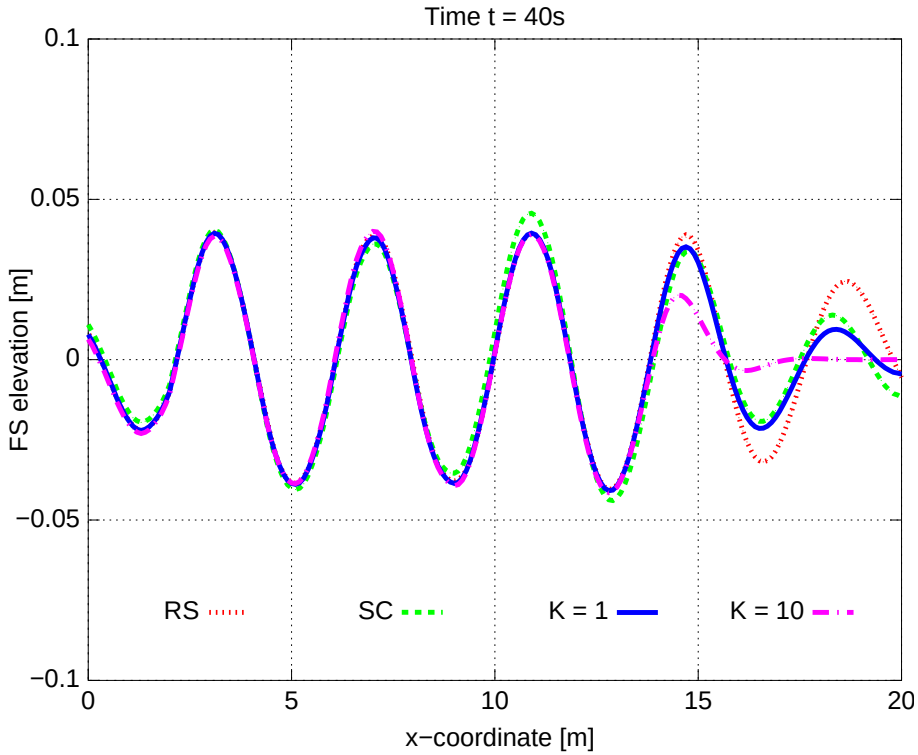

Figure 4: Open channel 3D. Free surface elevation for the RS, the solution SC, and the last two solved with AL, in time $t = 40$ s.

1. Using an extended domain $L_T = 3L$, as a reference solution (RS);

2. Without special treatment of the artificial boundary, with a domain length L, where a slip condition is used (SC);

3. With an absorbing layer (AL), considering two different K values over $L_a = 2\ \lambda = 7.75$ m, see Fig. 3, and a transition length $\gamma = \lambda = 3.873$ m.

The solution over the 3D domain was obtained for a mesh with hexahedral elements of $h_e = 0.10$ m each side, for a time step of $\Delta t = 0.025$ s and a final time of $T = 100$ s. The results obtained are shown in Figs. 4 to 6, for different times of simulation. The FS elevation is measured in the top nodes situated in longitudinal-vertical plane placed at 0.20 m from the lateral of the domain.

Note that the results are very similar to those obtained in Battaglia et al. (2011) for the 2D case. Furthermore, it is verified that due to the periodic conditions imposed in the longitudinal-vertical sides parallel to ABCD, the flow has a 2D behavior, as shown in Fig. 7.

The maximum FS displacement from time $t = 20$ s to time $t = 100$ s with respect of the x-position of the nodes is represented in Fig. 8, for all the four numerically solved cases: the reference solution (RS), the solution in the short domain with slip conditions (SC), and the two cases with AL, $K = 1$ and $K = 10$. The estimated decay of the FS amplitude of displacement are also represented in the γ part of the absorbing region, where K varies from 0 to the maximum value, see Fig. 2. The comparison of the curves obtained with AL and the estimated decay curves shows that for $K = 10$ the FS behavior has good agreement with the theoretical one; in the case with $K = 1$ there remain standing waves, although their amplitude roughly follows the estimated decay.

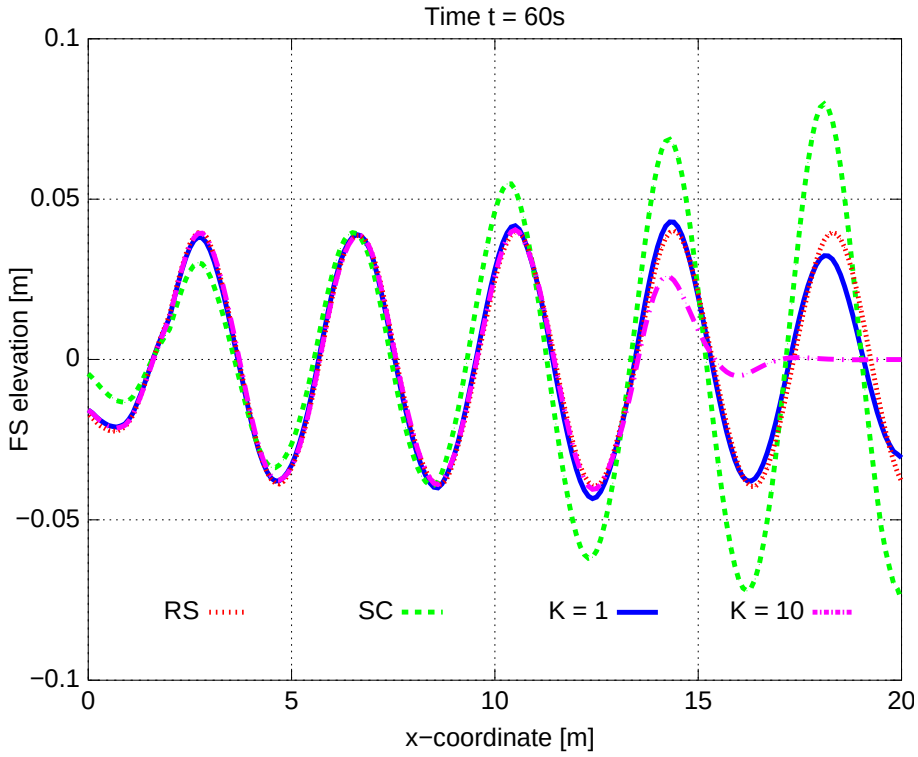

Figure 5: Open channel 3D. Free surface elevation for the RS, the solution SC, and the last two solved with AL, in time $t = 60$ s.

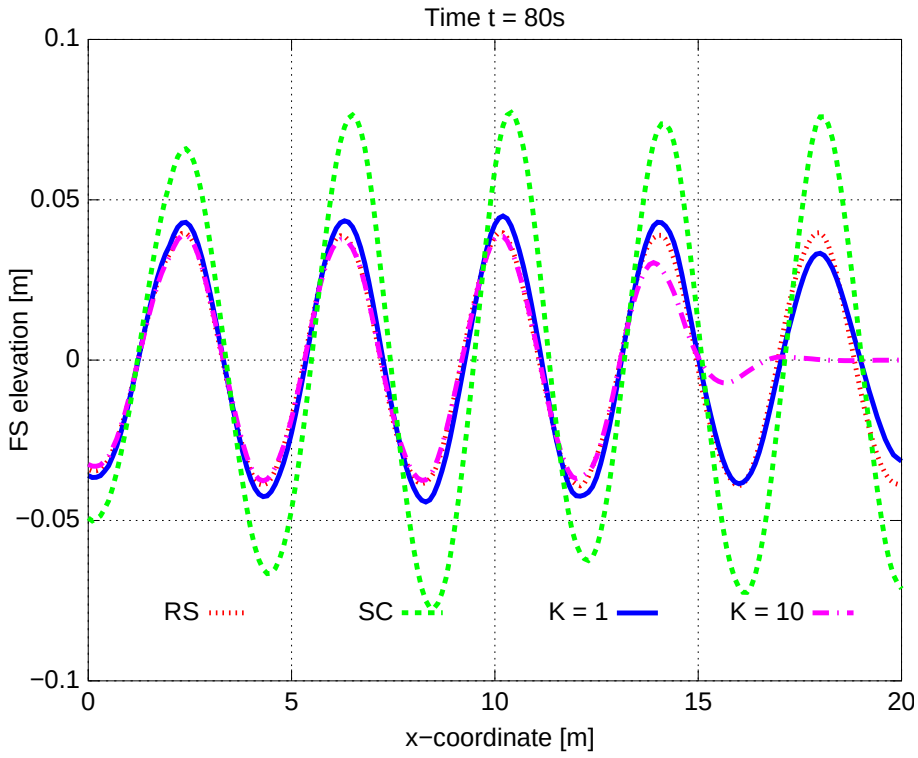

Figure 6: Open channel 3D. Free surface elevation for the RS, the solution SC, and the last two solved with AL, in time $t = 80$ s.

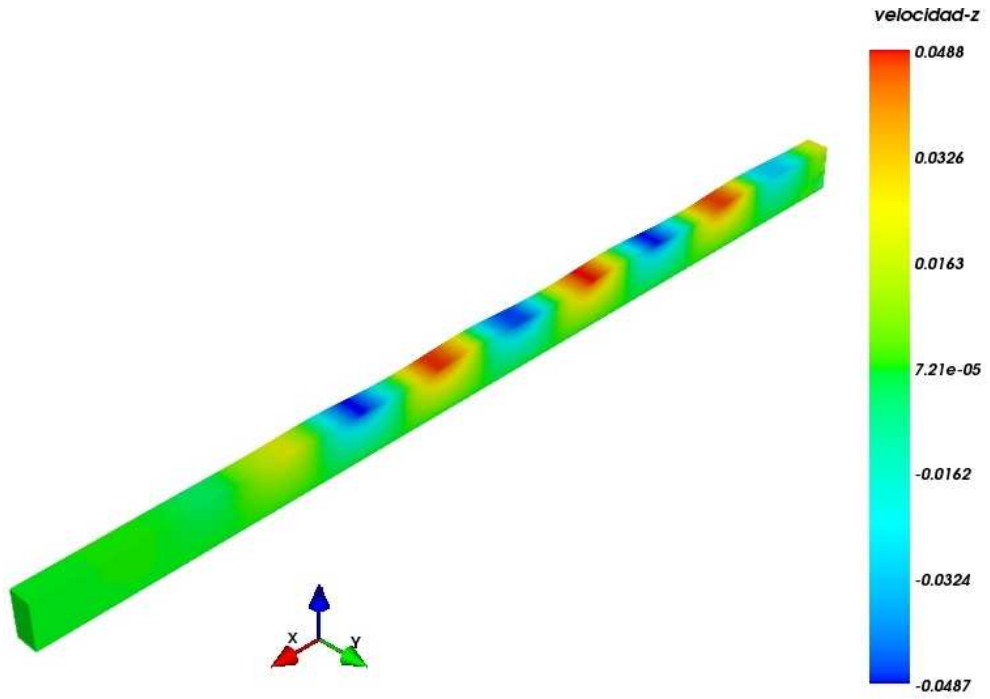

Figure 7: Open channel 3D. Vertical fluid velocities for the short domain solved with AL and $K = 10$.

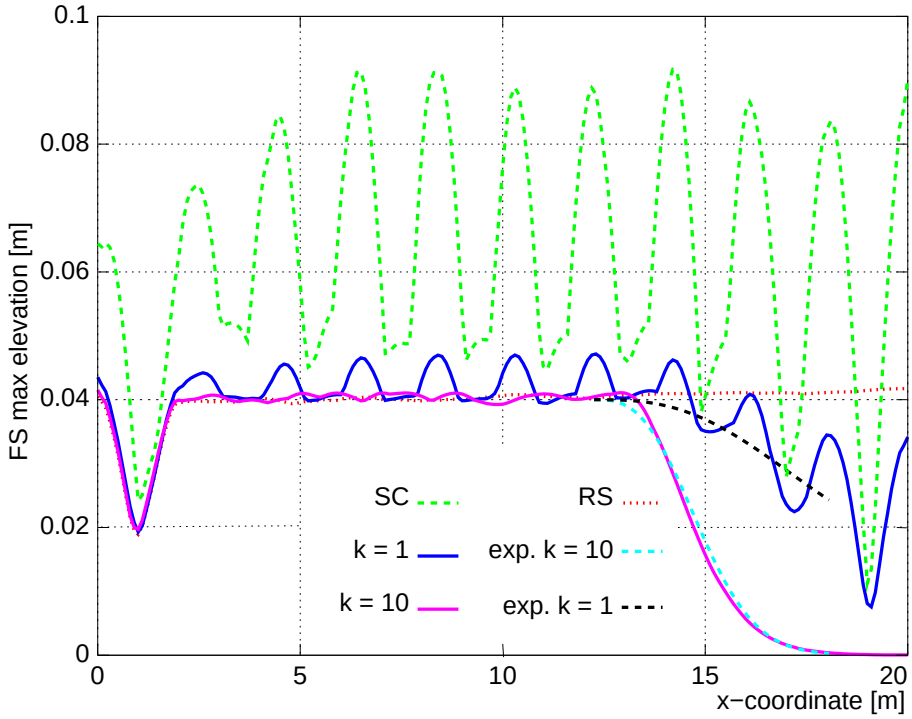

Figure 8: Open channel 3D. Maximum vertical displacements for each x-position from time $t = 20$ s to $t = 100$ s, for the RS, the SC, and the AL. The expected decay for $K = 1$ and $K = 10$ are sketched for the absorbing region with variable K, that is $12.25\ \mathrm{m} < \mathrm{x} < 18.06\ \mathrm{m}$.

4.2 Semi-infinite rectangular domain with wave generator

A 3D example is carried out over the domain sketched in Fig. 9, where the dimensions are $\mathrm{a} = 16$ m, $\mathrm{b} = 8$ m, $\mathrm{c} = \lambda/2 = 1.98$ m, and $\mathrm{d} = \lambda = 3.86$ m, with a fluid depth of $h_0 = 1$ m in z-direction. The rectangle defined by AGEF is the wave generator, and HBCJ represents the absorbing region.

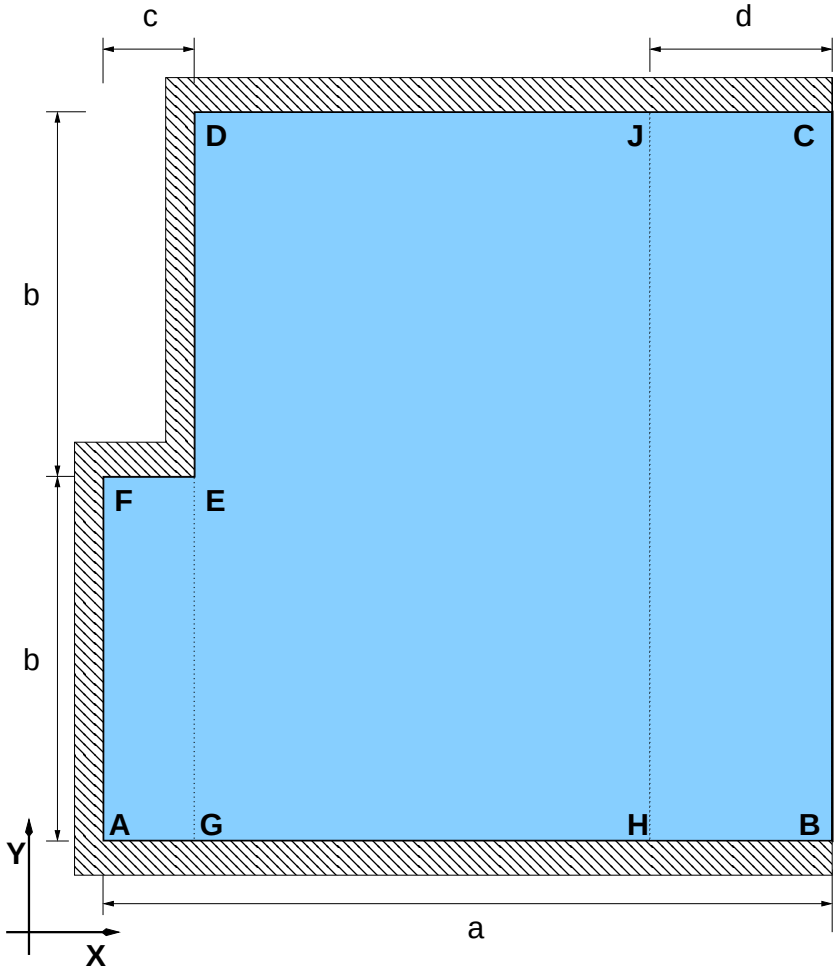

Figure 9: Rectangular domain with wave generation. Domain geometry in the horizontal plane.

For the whole contour, perfect slip conditions are given, including the artificial boundary BC, as well as for the bottom, while over the free surface is $P_{\text{atm}} = 0$, considering the NS problem. The fluid properties are kinematic viscosity $\nu = 1 \times 10^{-4}$ m^{2}s^{-1} and density $\rho = 1$ kg m^{-3}. The vertical component of the acceleration is $g_v = 1$ m s^{-2} for the whole domain, while the horizontal component for the wave generator in X-direction is given by Eq. (22) with a non-dimensional amplitude of $A = 0.06$. Furthermore, $c = \sqrt{g_v\, h} = 1$ m s^{-1} and the wavelength is $\lambda = 3.873$ m. For the MMV instance, the external contour ABCDEFA is free to move in vertical direction, the bottom is fixed, and the pseudo-elastic mesh update is used for the nodal positions update. The example is solved with and without AL, in order to establish a comparison between the FS behavior registered in each case.

The absorbing layer employed in this case is half of the one used for the former channel example, $L_a = \lambda = 3.873$ m. The variation of $K(x)$ from 0 to the maximum value takes the cubic variation shown in Fig. 2 for $\gamma = 0.75\ \lambda$. For the absorbing case, $K = 10$ was chosen.

The free surface stage is solved with the advective-diffusive module of the PETSc-FEM code, and requires a SUPG numerical stabilization procedure, taking into account the magnitude of the velocities and the FS displacements registered for this case, around 15% of the fluid depth, and about three times the amplitude of the previous example.

The mesh counts on hexahedral elements with a mean element size of $h_e = 0.20$ m, and the time step chosen is $\Delta t = 0.025$ s. Both the NS and the FS procedures were solved with $\theta = 0.5$ for the trapezoidal rule, and $4,000$ time steps were performed, using from 4 to 8 nodes of the Coyote cluster.

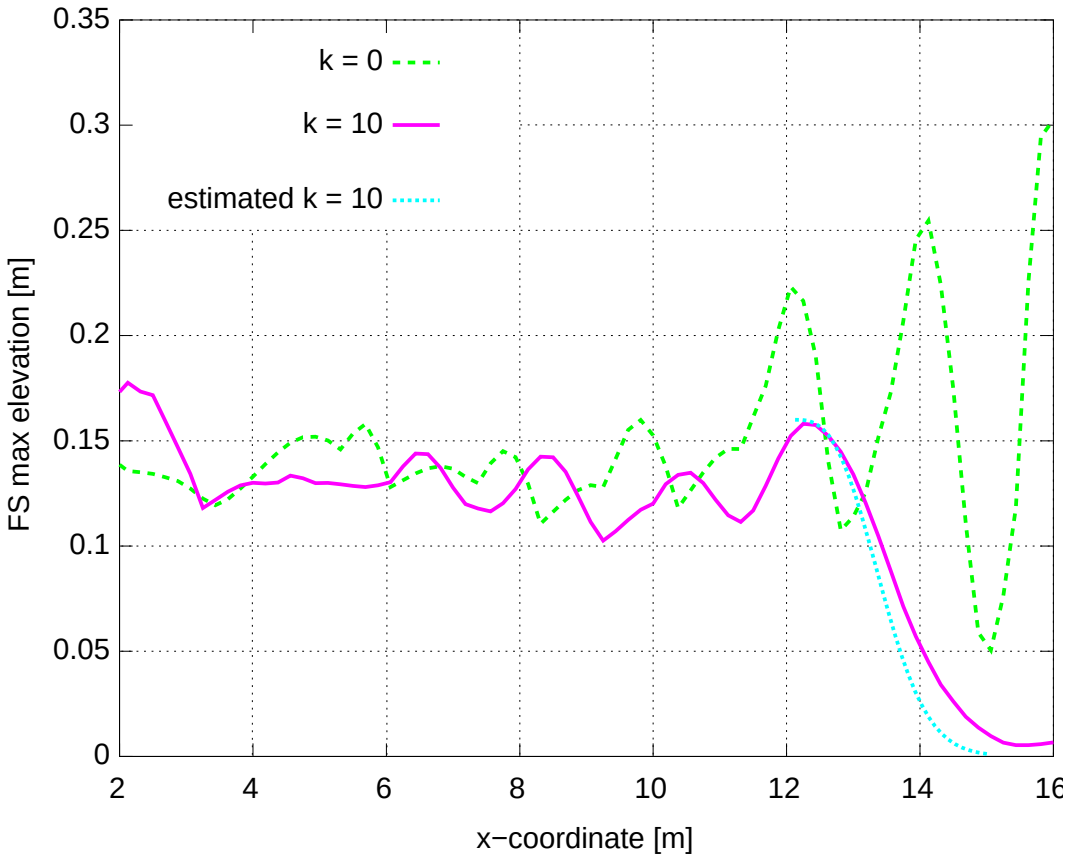

Figure 10: Rectangular domain with wave generation. Maximum wave amplitude over the side GB.

The maximum wave amplitude measured along the analysis over the side GB for each alternative is represented in Fig. 10. For the case without the AL, the analysis failed after 1740 time steps, with a total time of $t = 43.45$ s , and the amplitude reached 30% of the fluid depth near the artificial boundary $x = 16$ m in the graphics. The amplitude, that is expected to be quasi-uniform for pure traveling waves generated, shows the presence of standing waves. In the problem solved with $K = 10$, the amplitude is not constant neither, although the results are more uniform than those without absorption.

By comparison with the example of Sec. 4.1, the numerical solution with $K = 10$ does not decay as fast as the expected behavior, also represented in Fig. 10. The low absorption could be attributed to a low length of the absorbing layer L_a, together with the presence of waves that are not normal to the artificial boundaries, as those reflected in ED or DC.

The magnitude of the vertical velocity and the free-surface shape for different time steps, with and without AL, are represented in Figs. 11 and 12, respectively. In the case solved without

AL, Fig. 11, the graphics are given for times (a) $t = 27.5$ s, and (b) $t = 43.25$ s, where the last image is taken a few time steps before the analysis failure. For the same example solved with AL and $K = 10$, Fig. 12, three states are represented: (a) $t = 27.5$ s, (b) $t = 43.25$ s, and (c) $t = 67.5$ s. In Fig. 12 (a), there are not notorious differences with respect to the corresponding image of Fig. 11, while in (b) and (c) the absorbing effect in the AL can be appreciated, due to the decay of the amplitude of the displacements over the AL. In particular, for time $t = 43.25$ s, the velocities near the artificial contour are very different, see Figs. 11 (b) and 12 (b). At last, Fig. 12 (c) shows a FS pattern where the displacements are of the same order than in (b), and waves reflected over the artificial contour are not appreciated, although there are waves reflected over the CD side of the domain that arrive with an oblique angle with respect to the side BC.

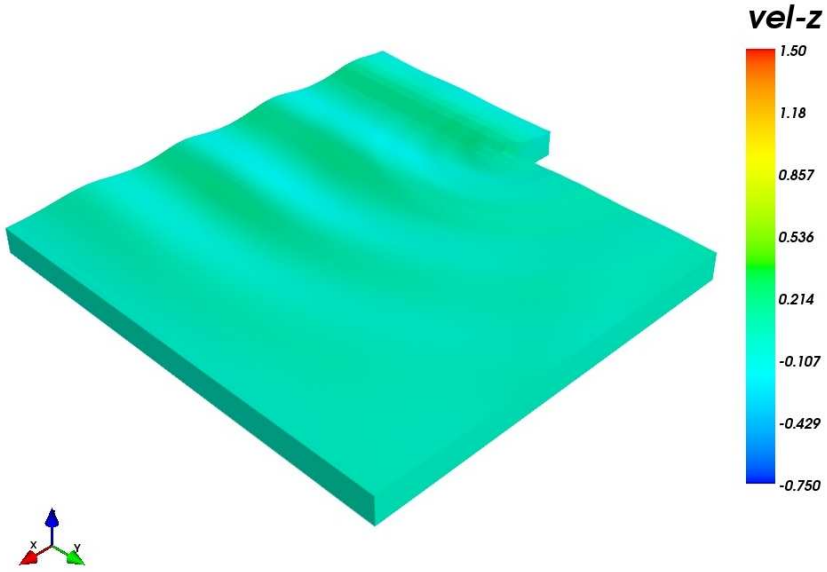

(a) Time $t = 27.5$ s

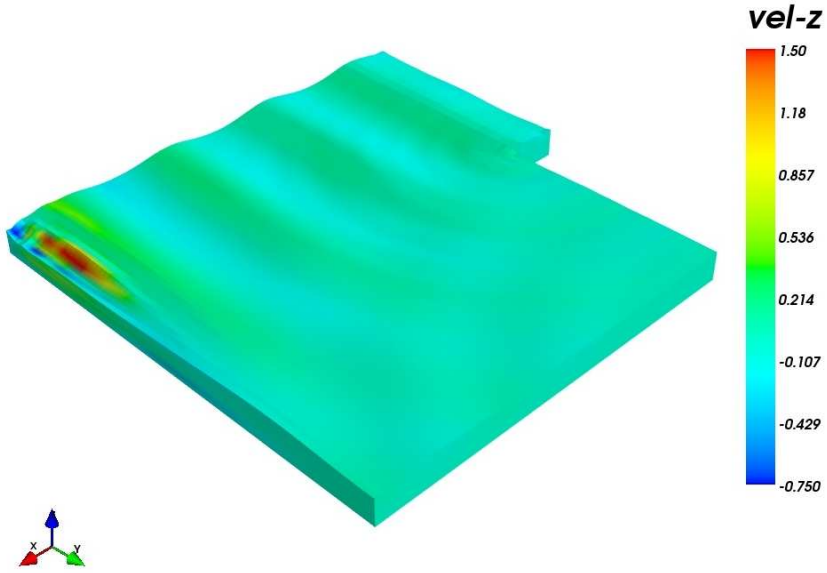

(b) Time $t = 43.25$ s

Figure 11: Rectangular domain with wave generation. Vertical velocity and free surface displacement without absorbing layer.

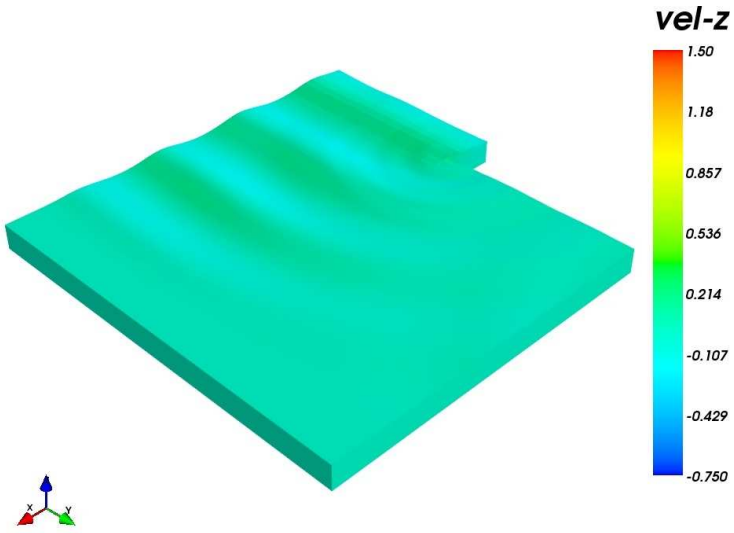

(a) Time $t = 27.5$ s

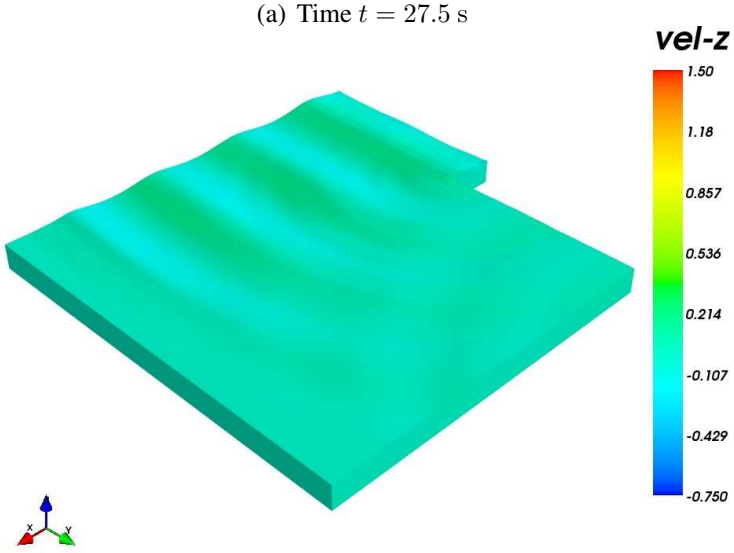

(b) Time $t = 43.25$ s

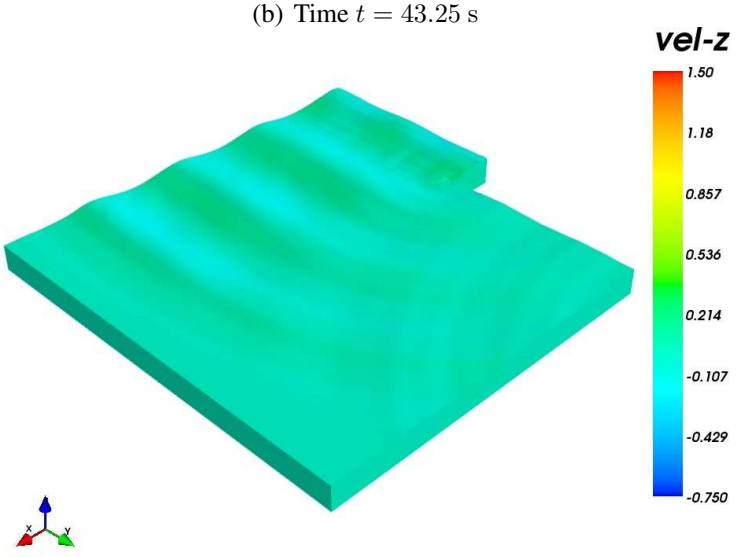

(c) Time $t = 67.5$ s

Figure 12: Rectangular domain with wave generation. Vertical velocity and free surface displacement with absorbing layer, $K = 10$.

5 CONCLUSIONS

An absorbing layer for solving FS fluid flows with artificial boundary conditions in 3D has been proposed, considering an ALE strategy. The methodology is based on the resolution of the shallow water equations, as detailed in Sec. 3. The numerical examples, without a mean current, show that the use of absorbing regions diminishes the spurious FS oscillations due to the reflection of the waves over the artificial boundary, in a magnitude that depends on the maximum value proposed for the penalization coefficient K, and on the width of the absorbing layer.

Acknowledgments This work has received financial support from Consejo Nacional de Investigaciones Científicas y Técnicas (CONICET, Argentina), Universidad Nacional del Litoral (UNL, Argentina, grants CAI+D 65-334/2009, CAI+D III-4-2/2009) and Agencia Nacional de Promoción Científica y Tecnológica (ANPCyT, Argentina, grants PICT 0270/2008, PICT 01141/2007, PICT 2492/2010), and was partially performed with the *Free Software Foundation GNU-Project* resources as GNU/Linux OS and GNU/Octave, as well as other Open Source resources as PETSc, MPICH, Paraview, LaTeX and JabRef.

REFERENCES

Balay S., Buschelman K., Eijkhout V., Gropp W., Kaushik D., Knepley M., McInnes L., Smith B., and Zhang H. PETSc Users Manual. ANL 95/11 - Revision 3.0.0, Argonne National Laboratory, 2008.

Battaglia L., D' Elía J., Storti M.A., and Nigro N.M. Numerical simulation of transient free surface flows using a moving mesh technique. *ASME Journal of Applied Mechanics*, 73(6):1017–1025, 2006. doi:10.1115/1.2198246.

Battaglia L., D'Elía J., and Storti M.A. Simulación numérica de la agitación en tanques de almacenamiento de líquidos mediante una estrategia lagrangiana euleriana arbitraria. *Revista Internacional de Métodos Numéricos para Cálculo y Diseño en Ingeniería*, 28(2):124–134, 2012. doi:10.1016/j.rimni.2012.02.001.

Battaglia L., Storti M., and D'Elía J. Interface-tracking free-surface flows in open domains. In O. Möller, J. Signorelli, and M. Storti, editors, *Mecánica Computacional*, volume XXX, pages 2209–2223. 2011.

Brooks A. and Hughes T.J.R. Streamline upwind/Petrov-Galerkin formulations for convection dominated flows with particular emphasis on the incompressible Navier-Stokes equations. *Computer Methods in Applied Mechanics Engineering*, 32(1-3):199–259, 1982. doi:10.1016/0045-7825(82)90071-8.

Clément A. Coupling of two absorbing boundary conditions for 2D time-domain simulations of free surface gravity waves. *Journal of Computational Physics*, 126(1):139 – 151, 1996. ISSN 0021-9991. doi:10.1006/jcph.1996.0126.

Colonius T. Modeling artificial boundary conditions for compressible flow. *Annual Review of Fluid Mechanics*, 36:315–345, 2004. doi:10.1146/annurev.fluid.36.050802.121930.

Coyote. The Coyote cluster at CIMEC. 2012. http://www.cimec.org.ar/twiki/bin/view/Cimec/-CoyoteCluster.

Güler I., Behr M., and Tezduyar T.E. Parallel finite element computation of free-surface flows. *Computational Mechanics*, 23(2):117–123, 1999. doi:10.1007/s004660050391.

Hughes T.J.R., Liu W.K., and Zimmermann T.K. Lagrangian-Eulerian finite element formu-

lation for incompressible viscous flows. *Computer Methods in Applied Mechanics and Engineering*, 29(3):329–349, 1981. doi:10.1016/0045-7825(81)90049-9.

López E.J., Nigro N.M., Storti M.A., and Toth J.A. A minimal element distortion strategy for computational mesh dynamics. *International Journal for Numerical Methods in Engineering*, 69(9):1898–1929, 2007.

MPI. Message Passing Interface. http://www.mcs.anl.gov/research/projects/mpi/, 2012.

Paz R.R., Storti M.A., and Garelli L. Local absorbent boundary condition for non-linear hyperbolic problems with unknown Riemann invariants. *Computers & Fluids*, 40(1):52 – 67, 2011. doi:10.1016/j.compfluid.2010.08.001.

PETSc-FEM. A general purpose, parallel, multi-physics FEM program. 2012. GNU General Public License (GPL).

Storti M.A. Absorbing boundary conditions for compressible flow at low Mach number and free surface flows with level set. Technical Report, Centro Internacional de Métodos Computacionales en Ingeniería (CIMEC), 2011.

Storti M.A., Nigro N.M., Paz R.R., and Dalcín L.D. Dynamic boundary conditions in computational fluid dynamics. *Computer Methods in Applied Mechanics Engineering*, 197(13–16):1219–1232, 2008. doi:10.1016/j.cma.2007.10.014. Elsevier, Amsterdam, The Netherlands.

Tezduyar T.E., Mittal S., Ray S.E., and Shih R. Incompressible flow computations with stabilized bilinear and linear-equal-order interpolation velocity-pressure elements. *Computer Methods in Applied Mechanics and Engineering*, 95(2):221–242, 1992. doi: 10.1016/0045-7825(92)90141-6.